



HAL
open science

Photochemical multivariate curve resolution models for the investigation of photochromic systems under continuous irradiation

O. Devos, H. Schröder, Michel Sliwa, J.P. Placial, K. Neymeyr, R. Métivier,
C. Ruckebusch

► To cite this version:

O. Devos, H. Schröder, Michel Sliwa, J.P. Placial, K. Neymeyr, et al.. Photochemical multivariate curve resolution models for the investigation of photochromic systems under continuous irradiation. *Analytica Chimica Acta*, 2019, 1053, pp.32-42. 10.1016/j.aca.2018.12.004 . hal-02412656

HAL Id: hal-02412656

<https://hal.science/hal-02412656>

Submitted on 21 Oct 2021

HAL is a multi-disciplinary open access archive for the deposit and dissemination of scientific research documents, whether they are published or not. The documents may come from teaching and research institutions in France or abroad, or from public or private research centers.

L'archive ouverte pluridisciplinaire **HAL**, est destinée au dépôt et à la diffusion de documents scientifiques de niveau recherche, publiés ou non, émanant des établissements d'enseignement et de recherche français ou étrangers, des laboratoires publics ou privés.



Distributed under a Creative Commons Attribution - NonCommercial 4.0 International License

Photochemical multivariate curve resolution models for the investigation of photochromic systems under continuous irradiation

O. Devos^{1*}, H. Schröder^{2,3}, M. Sliwa¹, J.P. Placial⁴,
K. Neymeyr^{2,3}, R. Métivier⁴, C. Ruckebusch^{1*}

¹ *Univ. Lille, CNRS, UMR 8516 - LASIR - Laboratoire de Spectrochimie Infrarouge et Raman, 59000 Lille, France*

² *Universität Rostock, Institut für Mathematik, Ulmenstrasse 69, 18057 Rostock, Germany*

³ *Leibniz-Institut für Katalyse, Albert-Einstein-Strasse 29a, 18059 Rostock, Germany*

⁴ *PPSM, ENS Cachan, CNRS, Université Paris-Saclay, Cachan, France*

** Corresponding author:*

olivier.devos@univ-lille.fr, +33 (0)3 20 43 47 48

Abstract

We propose a multivariate curve resolution approach for the investigation of photochromic systems using UV-Visible spectroscopy. The incorporation of photochemical hard-models as constraints in multivariate curve resolution alternating least squares (MCR-ALS) allows extracting reaction quantum yields in situations where a complete knowledge of the system is not available. We apply this approach to the study of the photochromism of CMTE (cis-1,2-dicyano-1,2-bis(2,4,5-trimethyl-3-thienyl)ethene) under continuous monochromatic irradiation. The mechanism, involving 3 species and 2 reversible reactions, are written and translated into a kinetic constraint that can be applied to the concentration profiles within ALS. For single set analysis, ambiguity of the solution obtained for photochemical model(s) is calculated and discussed. Multiset analysis is then proposed combining data obtained under different irradiation wavelengths to provide more reliable results. Finally, the photochemical reactivity of CMTE under different wavelengths is widely unraveled, and some description of the mechanism observed under irradiation at 365 nm is given.

Keywords (max. 6):

Photochemical reaction, Quantum yield, Multivariate curve resolution, Parameter ambiguity, Hard–soft modelling.

1. Introduction

Photochemical processes [1] are induced by light and occur in the excited states of molecules. They overcome large activation barriers yielding reactions that are often inaccessible by thermal processes.

Photochromic systems represent a class of photochemical compounds that can, upon photoirradiation, undergo reversible transformations between two different isomers of a molecule associated with different absorption spectra. In particular, diarylethenes[2] are photochromic molecules showing reversible photo-induced transformation between two different states, namely an open-form and a closed-form. This property opens wide fields of applications involving optical switching, such as opto(bio)electronic materials[3], optical triggers[4], photo-catalysis[5], optical data storage[6,7] or super-resolution imaging[8]. Although diarylethenes have been studied for more than 25 years, some aspects of their photochemistry are still unknown, and require more systematic quantitative analysis of their photokinetics and reaction mechanisms. Cis-1,2-dicyano-1,2-bis(2,4,5-trimethyl-3-thienyl)ethene, abbreviated CMTE (see **Scheme 1**), which was the first diarylethene to show stable and reversible photocyclization, is a typical example of a system involving different isomers with interconnected photoreactions[9,10].

The dynamics of photochemical systems is often investigated with UV-Visible spectroscopy under continuous monochromatic irradiation. One major issue concerns the quantification of the photochromic transformations, with the accurate determination of quantum yields related to the efficiency of unimolecular photoreactions[11], which are wavelength dependent parameters, and molar absorption spectra of the different species. Hard-modelling methods can be used for fitting photochemical processes. However, the situation is more complicated than for conventional kinetic hard-modelling. Indeed, in most

of the situations, all the involved species absorb irradiation UV light and compete each other, which translates into the introduction of a “photokinetic factor”. The corresponding set of non-autonomous linear differential equations can, generally speaking, only be solved numerically.

An alternative to hard modelling is multivariate curve resolution – alternating least squares (MCR–ALS)[12,13], a method that integrates chemical knowledge through constraints applied to the kinetic or spectral profiles. It has revealed a very useful approach to investigate complex spectrokinetic systems[14–17]. In addition, MCR-ALS allows combining multiple data sets from different experiments and/or different techniques [18–20] to provide more comprehensive and more accurate description of the chemical system under study. As an additional value to multiset analysis, kinetic hard-modelling analysis [21–23] can be applied as constraint on the concentration profiles. In time-resolved transient absorption spectroscopy for example, this approach was applied to photochromic reactions in situations where quantum yields are known (fixing the branching ratio of the photoproducts) [15,17]. The clear advantage of this so-called hard- and soft-modelling MCR is that it can handle situations where a complete knowledge of the system (reaction pathway, transient species formation process...) is not available, as when multiple excitation wavelength are used to investigate CMTE under continuous irradiation at different excitation wavelengths. In a more general view, the proposed approach is applicable to a wide range of photochromic systems for which complete tangible information is not available under the form of individual differential equations.

When using MCR techniques, as for factor analysis, it should always be considered the intrinsic limitation due to non-uniqueness of the pure component decomposition. This fact is known under the keyword rotational ambiguity [24–26]. The restriction of possible concentration factors by the use of a kinetic model does not guarantee a unique solution

[27,28]. The remaining ambiguity has been systematically analyzed for arbitrary first-order kinetic models [29]. A representation of this ambiguity by the parameters of the kinetic model, namely the set of feasible model parameters K^+ , has been proposed. A kinetic model parametrized by any element of K^+ is consistent with the concentration profiles and with the spectra, which together reconstruct the given spectroscopic data set. Thus, the set K^+ is an efficient tool to evaluate the ambiguity of the possible non-negative solutions of the MCR problem under the constraint of a kinetic model.

In this work, we propose a methodology for the analysis of a complex photochromic reaction scheme using MCR-ALS. This approach can potentially encompass a large variety of molecular mechanisms of photochemical and photochromic reactions. The photochromic behavior of CMTE (cis-1,2-dicyano-1,2-bis(2,4,5-trimethyl-3-thienyl)ethene) is chosen as a representative example of complex photochemical system which involves multiple, parallel, reversible and partially unknown reaction mechanisms. These mechanisms are written and translated into a hard-model constraint applied to the concentration profiles. Ambiguities of the solution obtained are calculated and discussed. The complete photochemical reactivity of CMTE is unraveled through a hard- and soft- multiset MCR approach.

2. Materials and methods / Experimental

2.1. Description of the CMTE system

CTME (cis-1,2-dicyano-1,2-bis(2,4,5-trimethyl-3-thienyl)ethene) exists mainly under three different isomers. Interconversion from one form to the others is induced by light irradiation following the mechanism presented in **Scheme 1**.

The open cis isomer of CMTE (A) displays a conjugated electronic structure allowing a $[4n+2]$ photoinduced electrocyclization reaction leading to a closed-ring form (B)

corresponding to a 1,3-cyclohexadiene-like molecular configuration. In competition with this photocyclization, reversible photoisomerization of the open cis isomer (A) to the open trans isomer (C) can occur. Both A and C solutions are yellowish whereas B shows an intense red color.

2.2. Study of CMTE under continuous irradiation – experimental conditions

The photochromic reaction of CMTE is studied using continuous irradiation with a Hg/Xe lamp (200W, Hamamatsu Lightningcure LC6) equipped with narrow-band interference filters of appropriate wavelengths. The transmitted light was recorded on a CCD camera through a polychromator. UV-Visible absorption spectra of the CMTE solutions in non-degassed chloroform were recorded from 275 to 625 nm every 0.7 second.

Three different spectral lines of the Hg/Xe irradiation source were selected: 405 nm, which is classically used to study the CMTE photocyclization, 365 nm, where other reaction(s) can be expected and 546 nm to induce the photo-cycloreversion. The three CMTE isomers (A, B and C) absorb at 365 nm and 405 nm, whereas only B is excited at 546 nm.

The three isomers, namely A, B and C, have been prepared from the commercially available CMTE (B1536 from Tokyo Chemical Industry Co., Ltd.). The purchased compound is initially in its A form. Under prolonged UV irradiation of a concentrated solution in chloroform, the B and C isomers have been isolated and purified by column chromatography, then unambiguously identified by X-ray crystallography[30]. Using pure A, B and C isomers as starting materials for photokinetic investigations, seven independent experiments were performed, varying the initial state or the irradiation wavelength, as described in **Table 1**. The corresponding spectra are shown in **Fig. 1**. We refer to reference [10] for further experimental details.

Under irradiation at 405 nm, both the reversible photocyclization and photocycloreversion ($A \rightarrow B$ and $B \rightarrow A$, respectively) and the *cis* \leftrightarrow *trans* photoisomerization ($A \rightarrow C$ and $C \rightarrow A$) occur. Therefore a hard-modelling approach based on the photochemical model proposed in **Scheme 1** can be applied to fit the data and extract the corresponding quantum yields.

Under irradiation at 546 nm, only the $B \rightarrow A$ reaction is induced since the open form species (A and C) do not absorb at this wavelength. Also, as mentioned in the introduction, it should be noted that the efficiency (quantum yield) of the photoreaction is different from the one observed under irradiation at 405 nm.

Under irradiation at 365 nm, the appearance of a fourth photochromic species (denoted D in the following) has been observed and its chemical structure has been investigated by NMR [30]. Consequently, at least one additional reaction has to be considered to describe the formation of this new product. Indeed, the spectra (see **Fig. 1**) show clearly the appearance of an absorption band centered at 450 nm, which band does not correspond to any of the pure isomers A, B and C. This translates into the fact that the mechanism presented in **Scheme 1**, which is valid for irradiation at 405 nm, is incomplete for irradiation at 365 nm. Indeed, at least one new interconnected photochromic reaction forming the product D should be considered. However, any a priori mechanism can be postulated for the formation of D as photo-oxidation is highly probable, and experimental conditions do not allow to control the concentration of O_2 .

2.3. Dynamics of CMTE under continuous irradiation at 405 nm

The kinetic photochemical model of CMTE under continuous irradiation at 405 nm involves three species and two pure photochemical reversible reactions (see **Scheme 1b**): a photocyclisation / photocycloreversion $A \leftrightarrow B$ with the associated quantum yields $\phi_{A \rightarrow B}$

, $\phi_{B \rightarrow A}$ and a cis-trans photo-isomerization $A \leftrightarrow C$ with the associated quantum yields $\phi_{A \rightarrow C}$, $\phi_{C \rightarrow A}$. The quantum yield is defined as the number of events (e.g. photo-induced transformation) divided by the number of absorbed photons in a specific system. Classically, quantum yields can range from 0 to 1. The fundamental kinetic laws of photochemical reaction under continuous irradiation are presented in the Appendix A.

For the system under study (see **Scheme 1b**) the kinetics of formation for each elementary reaction [31] are provided in Eqs (1-4):

$$A \rightarrow B (\phi_{A \rightarrow B}) \quad v_1 = \phi_{A \rightarrow B} (I_{0,irr} F(t)) l \varepsilon_{irr,A} C_A(t) \quad (1)$$

$$B \rightarrow A (\phi_{B \rightarrow A}) \quad v_2 = \phi_{B \rightarrow A} (I_{0,irr} F(t)) l \varepsilon_{irr,B} C_B(t) \quad (2)$$

$$A \rightarrow C (\phi_{A \rightarrow C}) \quad v_3 = \phi_{A \rightarrow C} (I_{0,irr} F(t)) l \varepsilon_{irr,A} C_A(t) \quad (3)$$

$$C \rightarrow A (\phi_{C \rightarrow A}) \quad v_4 = \phi_{C \rightarrow A} (I_{0,irr} F(t)) l \varepsilon_{irr,C} C_C(t) \quad (4)$$

with ϕ the quantum yield for a given reaction, $I_{0,irr}$ the intensity of the irradiation light (mole of photons.L⁻¹.s⁻¹), $F(t)$ the photokinetic factor (from 0 to 2.3 see Eqn. A.4), ε_{irr} the molar absorption coefficients at the irradiation wavelength in L.mol⁻¹.cm⁻¹, l the optical path length in cm and $C(t)$ the concentrations of the species for a given time. Each parameter is labelled with the letter corresponding to the considered species (A, B or C).

The photokinetic factor can be obtained either numerically, if the molar absorption coefficients of all the absorbing species at the irradiation wavelength is known, or experimentally, by measuring the absorption time-profile at the irradiation wavelength (Abs_{irr}). In situations where the pure spectra of each species can be isolated, it is preferable to derive the absorbance from the molar absorption coefficients in order to

obtain $F(t)$. This avoids handling spectral perturbations related to scattering of the irradiation light.

Finally the kinetic equations for the concentration change for each species are given in Eqs (5-7):

$$\frac{dC_A(t)}{dt} = -\nu_1 + \nu_2 - \nu_3 + \nu_4 \quad (5)$$

$$\frac{dC_B(t)}{dt} = +\nu_1 - \nu_2 \quad (6)$$

$$\frac{dC_C(t)}{dt} = +\nu_3 - \nu_4 \quad (7)$$

Furthermore the three species obey the mass balance equation given in the following equation (Eq. 8):

$$C_A(t) + C_B(t) + C_C(t) = C_0 \quad (8)$$

The kinetic equations given above are non-autonomous linear differential equations with non-separable variables. There exists no simple analytical solution to these equations. Therefore, numerical integration using for example Euler or other Runge-Kutta methods [32] should be considered.

3. Data analysis

Multivariate curve resolution or factorization methods for spectroscopic data, which are based on the bilinear Beer-Lambert law, can be shortly summarized by Eq. 9:

$$\mathbf{D} = \mathbf{C} \times \mathbf{S}^T + \mathbf{E} \approx \mathbf{C} \times \mathbf{S}^T \quad (9)$$

where $\mathbf{D}(m \times n)$ is a given spectral data matrix and the concentration profiles $\mathbf{C}(m \times k)$ of the k pure contributions and the corresponding pure spectra $\mathbf{S}^T(k \times n)$ have to be determined. The residual matrix $\mathbf{E}(m \times n)$ is assumed to be close to the zero matrix and can often be neglected.

For a given non-negative factorization $\mathbf{D} = \mathbf{C} \times \mathbf{S}^T$ further factorizations can easily be determined by inserting an arbitrary regular matrix $\mathbf{T}(k \times k)$ and its inverse $\mathbf{D} = \mathbf{C} \times \mathbf{S}^T = (\mathbf{C}\mathbf{T}^{-1}) \times (\mathbf{T}\mathbf{S}^T)$. However $\mathbf{C}' = \mathbf{C}\mathbf{T}^{-1}$ and $\mathbf{S}' = \mathbf{T}\mathbf{S}^T$ are not necessarily non-negative matrices. The term rotational ambiguity expresses the fact that usually a continuum of regular matrices \mathbf{T} exists so that \mathbf{C}' and \mathbf{S}' are non-negative. The insertion of \mathbf{T} and its inverse in Eq. 9 does not affect the lack of fit. The ambiguity can be reduced by imposing soft and/or hard constraints on the factors.

Adaptation of hybrid hard and soft-modelling MCR to photochemical models is introduced in Section 3.1. Section 3.2 explicitly evaluates the rotational ambiguity not only under the non-negativity constraint but also under the constraint of consistency with a photokinetic model.

3.1. Implementation of photochemical reaction in hard- and soft-modelling MCR

Only a brief description of MCR-ALS is given since more comprehensive information can be found in the literature. [13,21,22] Optimization is realized using an iterative procedure and based on the alternating evaluation of \mathbf{C} and \mathbf{S}^T using least squares, with the

application of constraints (egs., non-negativity, unimodality, closure) on the concentration and spectra profiles. It starts from an initial estimate of C or S^T . The quality of the decomposition is assessed from the lack of fit (lof, in %) between the experimental data matrix D and the data reproduced from the product $C \cdot S^T$, defined as in Eq. (10)

$$\mathbf{lof}(\%) = \mathbf{100} \times \sqrt{\frac{\sum (\mathbf{d}_{i,j}^* - \mathbf{d}_{i,j})^2}{\sum \mathbf{d}_{i,j}^2}} \quad (10)$$

where $d_{i,j}$ is one element of the experimental matrix and $d_{i,j}^*$ is the analogous element of the reproduced data. Convergence is achieved when the relative difference in lof between two consecutive iterations goes below a threshold or calculation stops when the number of iterations exceeds a pre-defined value.

Hard–soft multivariate curve resolution method (HS-MCR) is an evolution of the soft-modelling algorithm including a kinetic hard-modelling constraint. It can be particularly relevant to reduce ambiguity, to confirm a reaction mechanism and to estimate kinetic rates. The principle of HS-MCR using a photochemical model is presented in **Scheme 2**.

At each iteration, the concentration profiles in C (calculated by least squares) are fitted, and then updated by the hard-model profiles, in C_{fit} . The fitting step is performed using a Newton–Gauss Levenberg-Marquardt-based algorithm, which aims to minimize the value of sum of squares (ssq) given in Eq. 11:

$$\mathbf{ssq} = \|\mathbf{C}_{fit} - \mathbf{C}\|_F^2 \quad (11)$$

For each dataset, the irradiation intensity $I_{0,irr}$, the optical path length for the monitored absorption (here 1 cm), the molar absorption coefficients at the irradiation wavelength ($\epsilon_{A,irr}$, $\epsilon_{B,irr}$, $\epsilon_{C,irr}$) and the initial concentrations should be provided ($C_A(t = 0)$, $C_B(t = 0)$, $C_C(t = 0)$). The profiles in C_{fit} are obtained, for each compound, by integration of the

differential equation using Euler's method (see section 2.3). The algorithm will return S^T , C and the optimized parameters of the photochemical hard-model, namely the quantum yields ϕ_{opt} . It should be noted that not all the profiles in C have to be fitted and that, in multiset experiments, model-based and model-free experiments/species can be considered together.

3.2. Approximation of the set of feasible quantum yields

The previous section describes the computation of a non-negative factorization $D = C \times S^T$ under the constraint of a given kinetic model. The solution of this problem comprises not only optimized factors C_{opt} and S_{opt} but also quantum yields ϕ_{opt} . Typical relative error indicators to evaluate a solution are the lack of fit (see Eq. 10) as well as:

- non-negativity of C : $\frac{\|\min(C_{opt}, 0)\|_F}{\|C_{opt}\|_F}$, (12)

- non-negativity of S : $\frac{\|\min(S_{opt}, 0)\|_F}{\|S_{opt}\|_F}$, (13)

- kinetic fit: $\frac{\|C_{opt} - C_{fit}(\phi_{opt})\|_F}{\|C_{opt}\|_F}$. (14)

The set of feasible quantum yields K^+ contains those quantum yields, such that the corresponding factors C , S and C_{fit} have comparably small error values for each of the indicators. In many cases the set K^+ can be derived analytically and it can also be computed numerically [29]. Here, we focus on the latter. The approach is based on the main theoretical results of [29] and is briefly summarized next. The system of ordinary differential equations of Section 2.3 (Equations 5-7) can be written in matrix form

$$\begin{pmatrix} \dot{C}_A(t) \\ \dot{C}_B(t) \\ \dot{C}_C(t) \end{pmatrix} = I_{0,irr} \cdot F(t) \cdot M(\phi) \cdot \begin{pmatrix} C_A(t) \\ C_B(t) \\ C_C(t) \end{pmatrix} \quad (15)$$

with a coefficient matrix M :

$$M(\phi) = \begin{pmatrix} -\phi_{A \rightarrow B} - \phi_{A \rightarrow C} & \phi_{B \rightarrow A} & \phi_{C \rightarrow A} \\ \phi_{A \rightarrow B} & -\phi_{B \rightarrow A} & 0 \\ \phi_{A \rightarrow C} & 0 & -\phi_{C \rightarrow A} \end{pmatrix} \begin{pmatrix} \varepsilon_{irr,A} & 0 & 0 \\ 0 & \varepsilon_{irr,B} & 0 \\ 0 & 0 & \varepsilon_{irr,C} \end{pmatrix} \quad (16)$$

Then, the set K^+ of feasible quantum yields can be obtained by the following steps:

1. Compute a solution $(C_{opt}, S_{opt}, \phi_{opt})$ and the reconstructed data matrix $D_r = C_{opt} \times S_{opt}^T$.
2. Calculate the three eigenvalues $\lambda_1 \leq \lambda_2 \leq \lambda_3$ of the 3-by-3 matrix $M(\phi_{opt})$.
3. Determine the set K containing all ϕ so that the matrix $M(\phi)$ has the eigenvalues λ_1, λ_2 and λ_3 .
4. For each ϕ in K a pair of factors $S = (C_{fit}(\phi))^+ \times D_r$ and $C = D_r \times (S^T)^+$ can be calculated. Therein $(S^T)^+$ is the pseudoinverse of S^T . Each factor S is evaluated using the non-negativity constraint. The set of feasible quantum yields K^+ is defined by those ϕ which satisfy this constraint within a predefined tolerance.

The third step is the most complex one. Numerically, the set K is approximated by a dense grid of representatives which belong to K . We use a grid search algorithm [33]. For each grid point ϕ the program has to compute the eigenvalues $\lambda'_1 \leq \lambda'_2 \leq \lambda'_3$ of the 3×3 matrix $M(\phi)$. If the relative error $\|\lambda - \lambda'\|/\|\lambda\|$ is larger than a preset tolerance, the grid point ϕ is neglected. As matrix eigenvalue problems are only to be solved for 3-by-3 matrices the computational costs are low.

The fourth step contains an important property of this approach. Mathematically, the reconstruction of the factors C and S is based on a truncated singular value decomposition of the reconstructed data matrix $D_r = U\Sigma V^T$. Then the transformation matrix given by $T = C_{fit}^+(U\Sigma)$ ensures that the factors $C = U\Sigma T^+$ and $S = TV^T$ are optimal in a least squares

sense with respect to the model fit error. Once again, the lack of fit is not changed in comparison to the reconstruction of D by C_{opt} and S_{opt} .

Once the set K^+ is determined, there are several options to proceed:

- The rotational ambiguity under the constraint of the photokinetic model can be evaluated graphically by plots of the profiles given by the columns of C and S^T for each $\phi \in K^+$.

- The set K^+ can be scanned for solutions with the smallest nonnegativity constraint value and/or model fit error.

- Further constraints, e.g. unimodality or smoothness, can be applied to the set K^+ .

4. Results and discussion

4.1. Single set analysis of C under continuous irradiation at 405nm (C405)

4.1.1. MCR results

Under irradiation at 405 nm all the species absorb and the spectral data are clearly a mixture of the three identified species, A, B and C. The largest spectral changes are observed when starting from the pure form C. For this reason, we first apply MCR-ALS to the data C405. The selected constraints are non-negativity of the concentration and spectra, and closure of the concentration profiles (initial concentrations are known, see **Table 1**). The results obtained are provided in **Fig. 2**. The residuals are mainly noise and the corresponding lack of fit (lof) is 0.31%. The concentration profiles clearly correspond to the disappearance of the reactant, yielding two products. The presence of an equilibrium at long times (known as photo-stationary state) is also clearly observed. The spectra of A and C look very similar which is expected considering their chemical nature (cis or trans isomers).

In a second step, the photochemical model provided in **Scheme 1** (see also section 2.3) is applied as a hard-modelling constraint in MCR. The results are provided in **Fig. 3**. In addition, the estimated quantum yields for the different reactions are: $\phi_{A \rightarrow B} = 0.1917 \pm 0.0005$; $\phi_{B \rightarrow A} = 0.1747 \pm 0.0012$; $\phi_{A \rightarrow C} = 0.1206 \pm 0.0004$; $\phi_{C \rightarrow A} = 0.4331 \pm 0.0005$. The uncertainty reported here corresponds to the fitting error of the hard-model parameters obtained at the last iteration of the ALS procedure. The corresponding lof is 0.38%. Compared to the previous results (see **Fig. 2**) the concentration of the species C at long times is small but non-zero, whereas the concentration profile of A shows a more pronounced decrease after 300 seconds. Only slight modifications are observed on the spectral profiles.

4.1.2. Evaluation of the parameter ambiguity by K^+

To investigate rotational ambiguity of the solution obtained applying HS-MCR on the data of C405, we compute the set K^+ of feasible quantum yields. The eigenvalues of $M(\phi_{\text{opt}})$ are $\lambda_1 = -1640.6$, $\lambda_2 = -525.6$ and $\lambda_3 = 0$. A grid search algorithm is applied in order to compute K . The MatLab implementation can be found in Appendix B. The grid is initialized with 70 equally-spaced points in the interval $[0, 1]$ along each axis. The tolerance value for the relative error $\|\lambda - \lambda'\|/\|\lambda\|$, which is used to check a grid point, is set to 0.015 (or 1.5%). The computation time is 8.3 seconds on a single core with 3.6GHz of an Intel i7- 4790 CPU. Sometimes multiple runs of the grid search algorithm are needed to obtain optimal results. If the tolerance value is set too low, then only a set of isolated points is found by the grid search algorithm. However we expect for this problem a smooth manifold of solutions, cf. [29]. On the other hand, for an increasing tolerance value the approximation of K^+ shows an increasing volume. The reader can experiment with the MatLab code in Appendix B. We recommend tolerance values in the interval $[0.005, 0.02]$. If the computing power is not a critical point, then more grid points and hence smaller error tolerances can be used. The final step reduces K to its subset K^+ . A tolerance value of 0.0035 (or 0.35%) for the non-negativity constraint of the spectra is used in order to take noise into account. The value is set slightly higher than the relative negativity of the spectra which are obtained by HS-MCR, see **Fig. 3**. The sets K and K^+ are shown in **Fig. 4**. The set K^+ of feasible quantum yields is highlighted in blue in **Fig. 4**. It can be observed that, despite the strong restriction of the ensemble of feasible MCR decomposition due to the application of a photochemical model, the solution obtained is non-unique and may be significant as observed for the quantum yield of the reaction $C \rightarrow A$.

The MCR solutions corresponding to the set K^+ can be translated in concentration profiles and spectra by calculating the factors C and S for each $\phi \in K^+$, as described in

Section 3.2. The feasible concentration profiles and spectra are provided in **Fig. 5**. Clear differences are observed, especially in terms of concentration profiles, as expected from the set of K^+ . Considering now the set of feasible absorption spectra (see Figure 5b), very small variations are obtained for species C. There is almost no ambiguity on the pure spectrum of C due its selective presence at the beginning of the reaction. By contrast, for the species A and B, which are never observed selectively, the situation is different. Their feasible spectra are, even under the application of a photochemical hard-model, significantly affected by ambiguity as seen from the different possible shapes and amplitudes that can be obtained. Also the selective region around 500 nm results in an almost unique concentration profile of the component B aside from positive multiples. This can be verified, for example, by application of an equal-maximum scaling (as often used in MCR computations). However, the constraint of consistency with a photokinetic model predicts a concentration profile of the component B. This additional information should not be ignored.

The ambiguity mentioned above can be reduced in different ways. The most direct consists of fixing (some or all of) the spectra of pure species, considering that they are known. Another possibility would be to fix the final concentration values of the different species, considering that the composition of the photostationary state is known. These two approaches require a priori complete knowledge of the investigated system, which is seldom the case when investigating (partially) unknown systems. Another possibility is to analyze simultaneously multiple datasets, combining the results from different experiments and/or different techniques [18–20].

4.2. Multi-set MCR analysis combining data obtained with different irradiation wavelengths

The three datasets obtained under irradiation at 405 nm (A405, B405 and C405) are combined in a multiset approach. At 405 nm, the photochemical mechanism is known and can be applied simultaneously to the three data sets. In order to further reduce ambiguity of the resolution, the data B546 is considered as well. For these data, the reaction starts from pure B, and only A is formed. This ensures selective observation of the contributions of these species. However, under irradiation at 546 nm, the quantum yield $\phi_{A \rightarrow B}$ is different from the one at 405 nm. For this reason, although the approach allows different photokinetic models to be applied in the same multiset, only non-negativity and closure constraints were applied for B546. The results obtained for the HS-MCR resolution of the multiset [B546; A405; B405; C405] are provided in **Fig. 6**. The lof is now 1.22%, which remains very low. The optimized quantum yields values for irradiation at 405 nm are now: $\phi_{A \rightarrow B} = 0.1882 \pm 0.0008$; $\phi_{B \rightarrow A} = 0.2138 \pm 0.0020$; $\phi_{A \rightarrow C} = 0.1146 \pm 0.0006$; $\phi_{C \rightarrow A} = 0.3390 \pm 0.0012$. These values are slightly different from the ones obtained on the single set C405, as they correspond to the optimization of a multiset data. The application of the ambiguity analysis of the quantum yields for the multiset [A405; B405; C405] (see **Fig. 7**) shows the impact on the set K^+ by adding further data sets. The colored part is equal to the set K^+ that is displayed in Fig. 4 for C405 data. By considering the non-negativity of A405 and C405 the set reduces to the subset marked in red and yellow. The set K^+ shrinks again if additionally the data set B405 is taken into account. The remaining ambiguity is displayed as red subset. By comparison to the results obtained for single set analysis (blue, red and yellow part in **Fig. 7**), ambiguity is reduced and the solution is more reliable for the multiset analysis.

4.3. Analysis of data under continuous irradiation at 365nm.

Starting from the previous resolution of the multiset [B546; A405; B405; C405], we analyzed the data obtained under irradiation at 365 nm, for which the photoproduct D is known to be formed by photoreaction with O₂ [30]. Three datasets are available starting from pure A, B or C (A365, B365, C365). As previously, closure of the concentration profiles, as well as non-negativity of those concentrations and spectra, can be applied as soft-modeling constraints. However, no simple unimolecular reaction model can be provided under irradiation at 365 nm as the experiment was performed under variable and uncontrolled concentration of O₂. The concentration and spectral profiles obtained with HS-MCR applied to the multiset [B546; A405; B405; C405; A365; B365; C365] are presented in **Fig. 8**. The photochemical model is only applied for the data corresponding to irradiation at 405 nm. The corresponding lof is 1.51% and the optimized quantum yields for the reaction at 405 nm are consistent with the ones obtained previously ($\phi_{A \rightarrow B} = 0.2016 \pm 0.0004$; $\phi_{B \rightarrow A} = 0.2054 \pm 0.0008$; $\phi_{A \rightarrow C} = 0.1228 \pm 0.0005$; $\phi_{C \rightarrow A} = 0.3639 \pm 0.0007$).

It is worth noting that the concentration profiles of B, as displayed in **Fig. 7**, contain much less noise as compared to other isomers, which is consistent with its spectral characteristics. Indeed, the spectrum of B shows a specific absorption band at long wavelengths (500-600 nm) without overlap with other species. Besides, the concentration profiles corresponding to the samples irradiated at 405 nm [A405; B405; C405] are much better defined due to the hard model applied to this subset of data.

It should first be noted that the concentration profiles for the data at 405 nm, for which the photochemical model has been imposed, as well as the spectral profiles of the species A, B and C do not show important change compared with the one obtained on [B546; A405; B405; C405]. Focusing now on the results obtained under irradiation at 365 nm, the

concentrations of the isomer B for A365, B365 and C365 are much smaller than the ones observed for the system under irradiation at 405 nm. From those concentration profiles, it can reasonably be stated that the species D is formed from B. Indeed, the concentration profile of D shows a monotone increase and does not seem to be involved in an equilibrium, as observed for other species. Moreover, in all situations under 365 nm irradiation, a first transient period corresponds to a relatively fast interconversion between the A, B and C isomers, followed by a second time-period for which a global depopulation of these three isomers occurs, leading to the progressive appearance of the D form. This general behavior is fully compatible with a slow irreversible photoreaction involving oxygen. Besides, the pure spectrum of D, as identified by the multiset HS-MCR analysis, is well-compatible with the postulated structure mentioned in our previous works [30]: the maximum of the first absorption band of D is located around 460 nm, which is intermediate between the A and C isomers (< 400nm) and the B isomer (520 nm). Actually, the D species is expected to have a closed-ring structure with an oxidized side-group, leading to a more extended conjugated π -electron system compared to A and C, but less than B. As a final confirmation of our methodology, the general spectrum shape of the D species is consistent with the photoproduct chemically isolated after 365 nm irradiation.

Finally, such an analysis provides extremely useful information concerning the quantum yields of the photochromic reactions involved with CMTE, which were not fully unraveled to date. Only few uncomplete quantum yields determination trials have been mentioned in previous studies, in different media, neglecting the C isomer and the D photoproduct [10,34]. We can consider that the quantum yield set of values provided by the HS-MCR methodology described here represent the first complete photoreactivity quantification of the CMTE compound, which is widely used from its discovery by Irie and coworkers, 30 years ago [35]. The sum of quantum yields of the A isomer $\phi_{A \rightarrow B} + \phi_{A \rightarrow C} = 0.3244$ is

below 0.5, as usually observed for the diarylethene derivatives because of the parallel (photochemically inactive) / antiparallel (photochemically active) conformational equilibrium of the open-form at room temperature. We must highlight that the three isomers A, B and C display relatively large photochromic quantum yields, ranging between 0.12 and 0.36, and none of them negligible under UV-visible illumination. Therefore, consideration of all species and pathways is fully required when the photoreactivity of CMTE is evaluated.

5. Concluding remarks

The use of photochemical models as constraints on the concentration profiles in MCR-ALS allows estimating quantum yields of complex reactions involving multiple species entering simultaneous or sequential reversible reactions. However, in this case, even when applying a hard-model constraint, the solution is significantly affected by rotational ambiguity and different combinations of quantum yields may reproduce the data equally-well. To emphasize this point, the set of feasible concentration and absorption spectral profiles was computed and ambiguity of the MCR solutions was visualized. It was then proposed considering the investigation of a multiset data, for which the photochemical model only partially holds due to the incomplete knowledge of the reaction mechanisms, in order to reduce ambiguity. This strategy allowed the complete description of the photochemistry of CMTE investigated with UV-Visible absorption spectroscopy under continuous monochromatic irradiation. The quantum yields of the reactions at 405 nm could be extracted, as well as the photo-kinetic profiles and the absorption spectra of the A, B and C compounds involved. In addition, the spectral and kinetic features of a new species D formed under irradiation at 365 nm were obtained, and the processes involved in its formation could be confirmed. Finally, it should be highlighted that the proposed

approach can potentially encompass a large variety of molecular mechanisms of photochemical and photochromic reactions.

Acknowledgements

Research conducted within the context of the Nano-synergetics French/Japanese International Associated Laboratory.

Appendix A.

Fundamental kinetic laws of photochemical reaction under continuous irradiation.

Laws of photochemistry state that for system involving only one photon, the rate of the photochemical reaction is proportional to the photon flux absorbed by the photoreactive species. For an elementary/single photochemical reaction ($A \rightarrow B$) the change in concentration of the reactant (A) can be written as:

$$\frac{dC_A(t)}{dt} = -\Phi_{A \rightarrow B} I_{Abs_{A,irr}} \quad (A.1)$$

Where $C_A(t)$ is the concentration of the species A at the time t, $I_{Abs_{A,irr}}$ (mole of photon. $L^{-1}.s^{-1}$) is the time-dependent irradiation light intensity absorbed by the reactant and $\Phi_{A \rightarrow B}$ is the quantum yield of the formation of the photoproduct B.

There is competition for the absorption of the incident photon flux between the various absorbing species present in the medium. In the general case $I_{abs_{A,irr}}$ can be express as a fraction of the total intensity absorbed by the solution as:

$$I_{Abs_{A,irr}} = \frac{Abs_{A,irr}}{Abs_{irr}} I_{Abs,irr} = \epsilon_{A,irr} l C_A(t) I_{0,irr} \left(\frac{1 - 10^{-Abs_{irr}}}{Abs_{irr}} \right) \quad (A.2)$$

Where $Abs_{A,irr}$ is the absorbance due to the absorption of A only and Abs_{irr} the absorbance of the solution (all the species) that can be measured, $\epsilon_{A,irr}$ is the molar absorption coefficient of A at the irradiation wavelength in $L.mol^{-1}.cm^{-1}$, l the optical path length for the absorbance monitoring in cm.

Finally combining Eq. (A.1) and Eq. (A.2) give the general expression for the photochemical rate law for the consumption of the photoactive species A for $A \rightarrow B$ under monochromatic irradiation in well stirred fluid solution:

$$\frac{dC_A(t)}{dt} = -\phi_{A \rightarrow B} \left(I_{0,irr} F(t) \right) l \varepsilon_{A,irr} C_A(t) \quad (A.3)$$

Where $F(t)$ is a time-dependent dimensionless term referred to as the photokinetic factor, which is expressed in the case of only A and B absorb as :

$$F(t) = \frac{(1-10^{-Abs_{irr}})}{Abs_{irr}} = \frac{\left(1-10^{-l(\varepsilon_{A,irr}C_A(t)+\varepsilon_{B,irr}C_B(t))} \right)}{l(\varepsilon_{A,irr}C_A(t)+\varepsilon_{B,irr}C_B(t))} \quad (A.4)$$

F may change between the two limits, 0 for infinite absorbance and 2.3 when the absorbance tends to 0. Therefore in a photochemical reaction, the reaction rate depends not only on the reactant concentrations but on the concentration of the photoproducts as well.

Appendix B.

The grid search algorithm for the approximation of K

A grid search algorithm can be used in order to compute an approximation of the set K.

The following MatLab code can be used for this purpose:

```
% extinction coefficients
E=[3.1075 1.0862 2.3365]*1E3;
%coefficient matrix
M=@(p) [-p(1)-p(3) p(2) p(4); p(1) -p(2) 0;p(3) 0 -p(4)]*
    diag(E);
%phi_opt
popt=[0.19107, 0.17417, 0.11962, 0.43293];
EW=sort(eig(M(popt)));
%dimension reduction
psum=sum(popt*diag(E([1 2 1 3])));

% #grid points
lenGS=70;
%tolerance
tol=0.015;

% grid search
v1=linspace(0,1,lenGS);
v3=linspace(0,1,lenGS);
v4=linspace(0,1,lenGS);
v2=@(v1,v3,v4) E(2)^(-1)*(psum-sum([v1 v3 v4]*diag(E([1 1
    3]))));
Acc=[];
for i=1:lenGS
    disp([num2str(100*i/lenGS,3) ' %'])
    for j=1:lenGS
        for k=1:lenGS
            pc=[v1(i) v2(v1(i),v3(j),v4(k)) v3(j) v4(k)];
            EWc=sort(eig(M(pc)));
            if norm(EWc-EW)/norm(EW)<=tol && min(pc)>=0
                Acc=[Acc [v1(i) v3(j) v4(k)]'];
            end
        end
    end
end
end
%plot
plot3(Acc(2,:),Acc(3,:),Acc(1,:), '*k')
view([-186 50])
axis tight
```

References

- [1] N.J. Turro, V. Ramamurthy, J.C. Scaiano, *Modern Molecular Photochemistry of Organic Molecules*, University Science Books, 2010.
<https://books.google.fr/books?id=31JCAQAIAAJ>.
- [2] M. Irie, T. Fukaminato, K. Matsuda, S. Kobatake, *Photochromism of Diarylethene Molecules and Crystals: Memories, Switches, and Actuators*, *Chem. Rev.* 114 (2014) 12174–12277. doi:10.1021/cr500249p.
- [3] F. Wang, X. Liu, I. Willner, *Integration of Photoswitchable Proteins, Photosynthetic Reaction Centers and Semiconductor/Biomolecule Hybrids with Electrode Supports for Optobioelectronic Applications*, *Adv. Mater.* 25 (n.d.) 349–377.
doi:10.1002/adma.201201772.
- [4] C. Bertarelli, A. Bianco, R. Castagna, G. Pariani, *Photochromism into optics: Opportunities to develop light-triggered optical elements*, *J. Photochem. Photobiol. C Photochem. Rev.* 12 (2011) 106–125. doi:10.1016/j.jphotochemrev.2011.05.003.
- [5] R.S. Stoll, S. Hecht, *Artificial Light-Gated Catalyst Systems*, *Angew. Chem. Int. Ed.* 49 (n.d.) 5054–5075. doi:10.1002/anie.201000146.
- [6] S. Luo, K. Chen, L. Cao, G. Liu, Q. He, G. Jin, D. Zeng, Y. Chen, *Photochromic diarylethene for rewritable holographic data storage*, *Opt. Express.* 13 (2005) 3123–3128.
doi:10.1364/OPEX.13.003123.
- [7] S. Kawata, Y. Kawata, *Three-Dimensional Optical Data Storage Using Photochromic Materials*, *Chem. Rev.* 100 (2000) 1777–1788. doi:10.1021/cr980073p.
- [8] O. Nevskiy, D. Sysoiev, J. Dreier, S.C. Stein, A. Oppermann, F. Lemken, T. Janke, J. Enderlein, I. Testa, T. Huhn, D. Wöll, *Fluorescent Diarylethene Photoswitches—A Universal Tool for Super-Resolution Microscopy in Nanostructured Materials*, *Small.* 14 (n.d.) 1703333. doi:10.1002/sml.201703333.
- [9] T. Kawai, T. Koshido, K. Yoshino, *Optical and dielectric properties of photochromic dye in amorphous state and its application*, *Appl. Phys. Lett.* 67 (1995) 795–797.
doi:10.1063/1.115470.
- [10] A. Spangenberg, J.A.P. Perez, A. Patra, J. Piard, A. Brosseau, R. Métivier, K. Nakatani, *Probing photochromic properties by correlation of UV-visible and infra-red absorption spectroscopy: a case study with cis-1,2-dicyano-1,2-bis(2,4,5-trimethyl-3-thienyl)ethene*, *Photochem. Photobiol. Sci.* 9 (2010) 188–193. doi:10.1039/B9PP00133F.
- [11] M.H. Deniel, D. Lavabre, J.C. Micheau, *Photokinetics under Continuous Irradiation*, in: J.C. Crano, R.J. Guglielmetti (Eds.), *Org. Photochromic Thermochromic Compd.*, Springer US, 2002: pp. 167–209. doi:10.1007/0-306-46912-X_4.
- [12] R. Tauler, *Multivariate curve resolution applied to second order data*, *Chemom. Intell. Lab. Syst.* 30 (1995) 133–146.
- [13] A. de Juan, R. Tauler, *Chapter 2 - Multivariate Curve Resolution-Alternating Least Squares for Spectroscopic Data*, in: C. Ruckebusch (Ed.), *Data Handl. Sci. Technol.*, Elsevier, 2016: pp. 5–51. doi:10.1016/B978-0-444-63638-6.00002-4.
- [14] N. Mouton, A. de Juan, M. Sliwa, C. Ruckebusch, *Hybrid hard- and soft-modeling approach for the resolution of convoluted femtosecond spectrokinetic data*, *Chemom. Intell. Lab. Syst.* 105 (2011) 74–82. doi:10.1016/j.chemolab.2010.11.002.
- [15] N. Mouton, O. Devos, M. Sliwa, A. de Juan, C. Ruckebusch, *Multivariate curve resolution – Alternating least squares applied to the investigation of ultrafast competitive photoreactions*, *Anal. Chim. Acta.* 788 (2013) 8–16. doi:10.1016/j.aca.2013.06.027.

- [16] C. Ruckebusch, L. Blanchet, Multivariate curve resolution: A review of advanced and tailored applications and challenges, *Anal. Chim. Acta.* 765 (2013) 28–36. doi:10.1016/j.aca.2012.12.028.
- [17] O. Devos, S. Aloïse, M. Sliwa, R. Métivier, J.-P. Placial, C. Ruckebusch, Chapter 11 - Multivariate Curve Resolution of (Ultra)Fast Photoinduced Process Spectroscopy Data, in: C. Ruckebusch (Ed.), *Data Handl. Sci. Technol.*, Elsevier, 2016: pp. 353–379. doi:10.1016/B978-0-444-63638-6.00011-5.
- [18] S. Mas, R. Tauler, A. de Juan, Chromatographic and spectroscopic data fusion analysis for interpretation of photodegradation processes, *J. Chromatogr. A.* 1218 (2011) 9260–9268. doi:10.1016/j.chroma.2011.10.035.
- [19] S. Navea, A. de Juan, R. Tauler, Modeling Temperature-Dependent Protein Structural Transitions by Combined Near-IR and Mid-IR Spectroscopies and Multivariate Curve Resolution, *Anal. Chem.* 75 (2003) 5592–5601. doi:10.1021/ac0343883.
- [20] C. Fernández, M. Pilar Callao, M. Soledad Larrechi, UV–visible-DAD and ¹H-NMR spectroscopy data fusion for studying the photodegradation process of azo-dyes using MCR-ALS, *Talanta.* 117 (2013) 75–80. doi:10.1016/j.talanta.2013.08.004.
- [21] A. de Juan, M. Maeder, M. Martínez, R. Tauler, Combining hard- and soft-modelling to solve kinetic problems, *Chemom. Intell. Lab. Syst.* 54 (2000) 123–141. doi:10.1016/S0169-7439(00)00112-x.
- [22] A. de Juan, M. Maeder, M. Martínez, R. Tauler, Application of a novel resolution approach combining soft- and hard-modelling features to investigate temperature-dependent kinetic processes, *Anal. Chim. Acta.* 442 (2001) 337–350. doi:10.1016/S0003-2670(01)01181-3.
- [23] L. Blanchet, C. Ruckebusch, J.-P. Huvenne, A. de Juan, Focus on the potential of hybrid hard- and soft-MCR–ALS in time resolved spectroscopy, *J. Chemom.* 22 (2008) 666–673. doi:10.1002/cem.1144.
- [24] E.R. Malinowski, *Factor Analysis in Chemistry*, 3rd Edition, Wiley, New York, 2002.
- [25] M. Maeder, Y.M. Neuhold, *Practical Data Analysis in Chemistry*, Elsevier Science, Amsterdam, 2007.
- [26] H. Abdollahi, R. Tauler, Uniqueness and rotation ambiguities in Multivariate Curve Resolution methods, *Chemom. Intell. Lab. Syst.* 108 (2011) 100–111. doi:10.1016/j.chemolab.2011.05.009.
- [27] N.W. Alcock, D.J. Benton, P. Moore, Kinetics of series first-order reactions. Analysis of spectrophotometric data by the method of least squares and an ambiguity, *Trans. Faraday Soc.* 66 (1970) 2210–2213. doi:10.1039/TF9706602210.
- [28] S. Vajda, H. Rabitz, Identifiability and distinguishability of first-order reaction systems, *J. Phys. Chem.* 92 (1988) 701–707. doi:10.1021/j100314a024.
- [29] H. Schröder, M. Sawall, C. Kubis, D. Selent, D. Hess, R. Franke, A. Börner, K. Neymeyr, On the ambiguity of the reaction rate constants in multivariate curve resolution for reversible first-order reaction systems, *Anal. Chim. Acta.* 927 (2016) 21–34. doi:10.1016/j.aca.2016.04.009.
- [30] F.G. Erko, J. Berthet, A. Patra, R. Guillot, K. Nakatani, R. Métivier, S. Delbaere, Spectral, Conformational and Photochemical Analyses of Photochromic Dithienylethene: cis-1,2-Dicyano-1,2-bis(2,4,5-trimethyl-3-thienyl)ethene Revisited, *Eur. J. Org. Chem.* 2013 (2013) 7809–7814. doi:10.1002/ejoc.201301143.

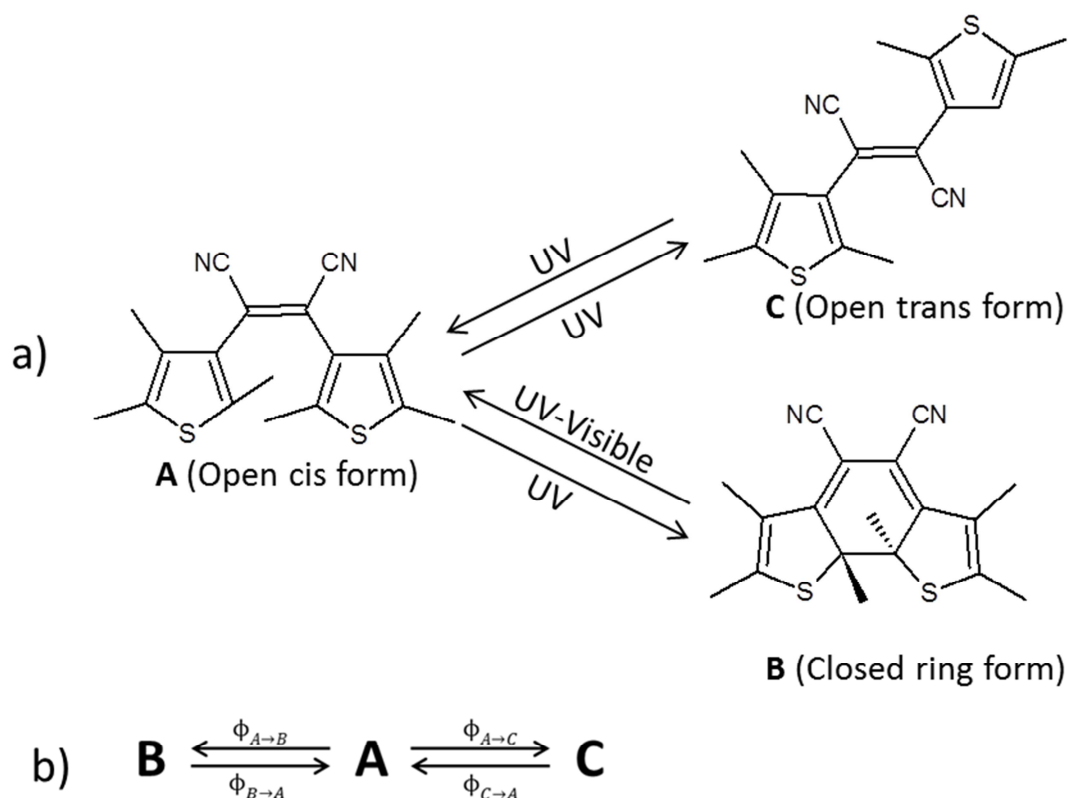
- [31] K. Nakatani, J. Piard, P. Yu, R. Métivier, Introduction: Organic Photochromic Molecules, in: *Photochromic Mater.*, Wiley-Blackwell, 2016: pp. 1–45.
doi:10.1002/9783527683734.ch1.
- [32] B.A. Barshop, R.F. Wrenn, C. Frieden, Analysis of numerical methods for computer simulation of kinetic processes: Development of KINSIM—A flexible, portable system, *Anal. Biochem.* 130 (1983) 134–145. doi:10.1016/0003-2697(83)90660-7.
- [33] Vosough Maryam, Mason Caroline, Tauler Romà, Jalali-Heravi Mehdi, Maeder Marcel, On rotational ambiguity in model-free analyses of multivariate data, *J. Chemom.* 20 (2007) 302–310. doi:10.1002/cem.1022.
- [34] H. Ishitobi, Z. Sekkat, M. Irie, S. Kawata, The Photoorientation Movement of a Diarylethene-Type Chromophore, *J. Am. Chem. Soc.* 122 (2000) 12802–12805.
doi:10.1021/ja002185f.
- [35] M. Irie, M. Mohri, Thermally irreversible photochromic systems. Reversible photocyclization of diarylethene derivatives, *J. Org. Chem.* 53 (1988) 803–808.
doi:10.1021/jo00239a022.

Table

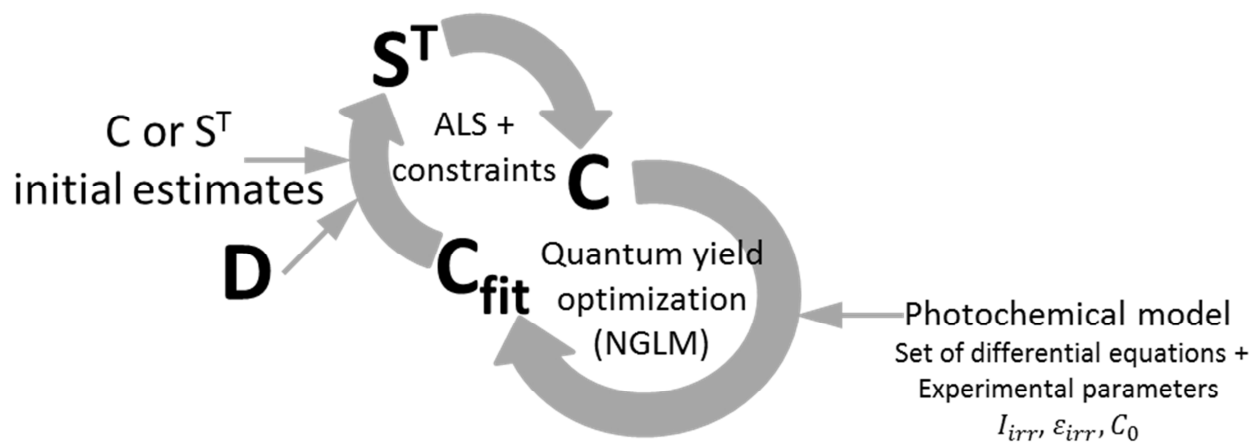
Name of the experiment	Initial state (conc. in mol.L ⁻¹)			Irradiation wavelength	Irradiation intensity (mole.L ⁻¹ .s ⁻¹)
	A	B	C		
B546	–	4.9×10 ⁻⁵	–	546 nm	5,2×10 ⁻⁶
A405	6.2×10 ⁻⁵	–	–	405 nm	4,8×10 ⁻⁶
B405	–	6.6×10 ⁻⁵	–	405 nm	5,1×10 ⁻⁶
C405	–	–	1.1×10 ⁻⁴	405 nm	4,5×10 ⁻⁶
A365	6.7×10 ⁻⁵	–	–	365 nm	
B365	–	7.4×10 ⁻⁵	–	365 nm	
C365	–	–	1.2×10 ⁻⁴	365 nm	

Table 1. Initial concentrations, irradiation wavelengths and intensity of the seven experiments.

Schemes



Scheme 1. a) Photochromic reaction mechanism of CMTE showing the reversible photocyclization and the cis/trans photoisomerization with b) a sequential photokinetic model.



Scheme 2: principle of HS-MCR including a photochemical model

Figures captions

Fig. 1. UV-Visible absorption spectra of the CMTE isomers (A, B and C) at different times under continuous irradiation at 405, 365 and 546 nm. Spectra were recorded every 0.7 second. The red spectra correspond to data acquired at the beginning of the process and the blue ones to the last spectra of the series.

Fig. 2. Kinetic concentration profiles and absorption spectra for data corresponding to irradiation at 405 nm starting from C, obtained applying MCR with only soft constraints (non-negativity and closure).

Fig. 3. Kinetic concentration profiles and absorption spectra for data corresponding to irradiation at 405 nm starting from C, obtained applying HS-MCR with the CMTE photochemical model, non-negativity on concentration and spectra and the closure constraints.

Fig. 4. Approximations of the sets K (a) and K+ (b); the quantum yields ϕ_{opt} obtained by MCR are marked as black cross in the two plots. The shading of K is used for visualization purpose. The non-negativity constraint of the factor S was applied with a tolerance of 0.35% in order to reduce K to K+. The set K+ is shown in blue color in the right plot. $\phi_{\text{(B}\rightarrow\text{A)}}$ is determined using the others quantum yields using the formula presented in the code in Appendix B (variable called v2).

Fig. 5. Plots of the bands of a) concentration profiles and b) absorption spectra. The feasible factors C and S are evaluated for each representative of the set K+, which is shown in Fig. 4.

Fig. 6. HS-MCR results (top: concentration profiles, bottom: absorption spectra) for the multiset data [B546; A405; B405; C405]. The CMTE photochemical model was applied for the data at 405 nm. Only non-negativity of the concentrations and absorption spectra and closure constraints were applied for the data at 546 nm.

Fig. 7. Approximations of the set K+ are shown for different multisets. First, the single data set C405 results in K+ as shown in blue, yellow and red. The set K+ for the multiset [A405; C405] is drawn in yellow and red. Finally, the largest multiset [A405; B405; C405] results in the smallest set K+ (red). The quantum yield vector ϕ_{opt} obtained by HS-MCR is marked by a black cross.

Fig. 8. HS-MCR results (top: concentration profiles, bottom: absorption spectra) for the multiset [B546; A405; B405; C405; A365; B365; C365]. The CMTE photochemical model was applied for the data at 405 nm. Only non-negativity of the concentrations and absorption spectra and closure constraints were applied for the data at 546 nm and 365 nm.

Figure 1

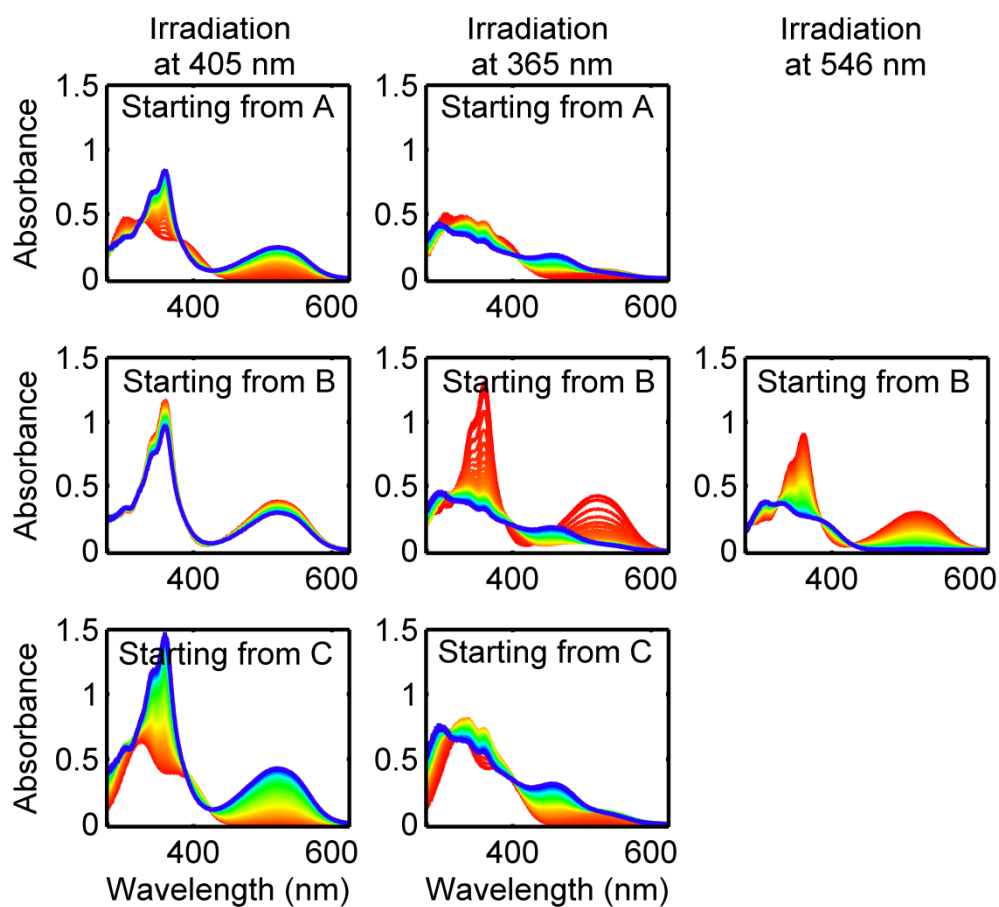


Fig. 1. UV-Visible absorption spectra of the CMTE isomers (A, B and C) at different times under continuous irradiation at 405, 365 and 546 nm. Spectra were recorded every 0.7 second. The red spectra correspond to data acquired at the beginning of the process and the blue ones to the last spectra of the series.

Figure 2

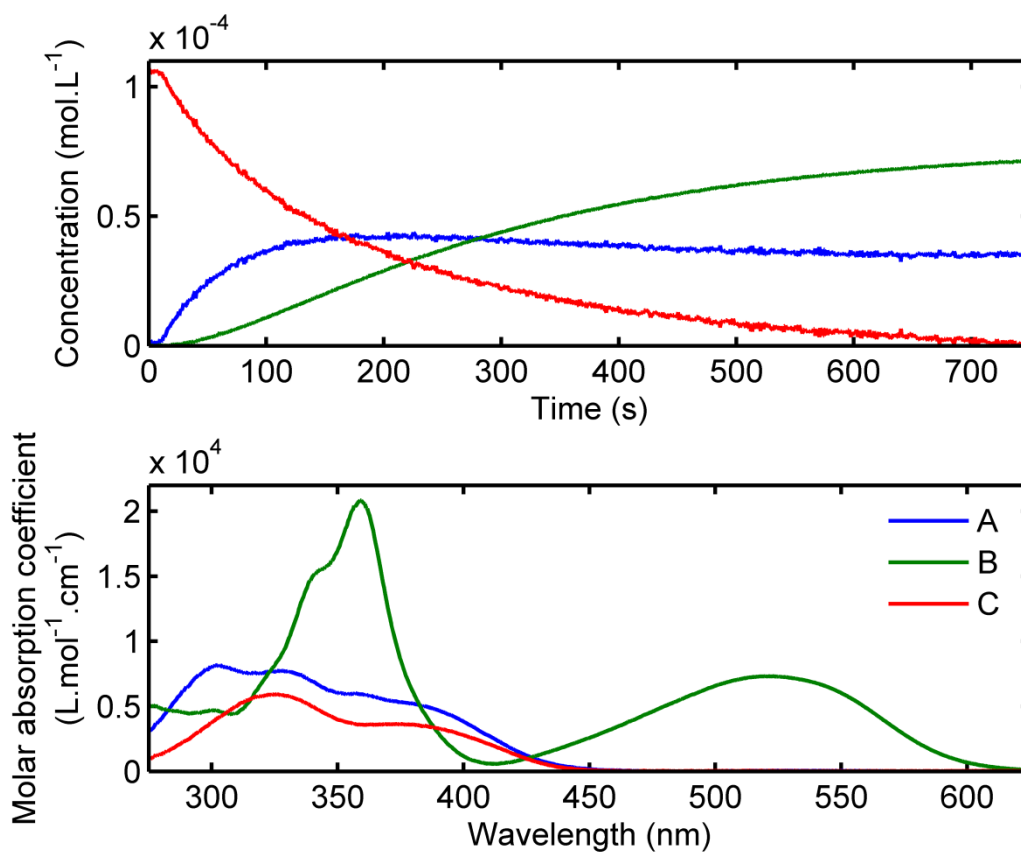


Fig. 2. Kinetic concentration profiles and absorption spectra for data corresponding to irradiation at 405 nm starting from C, obtained applying MCR with only soft constraints (non-negativity and closure).

Figure 3

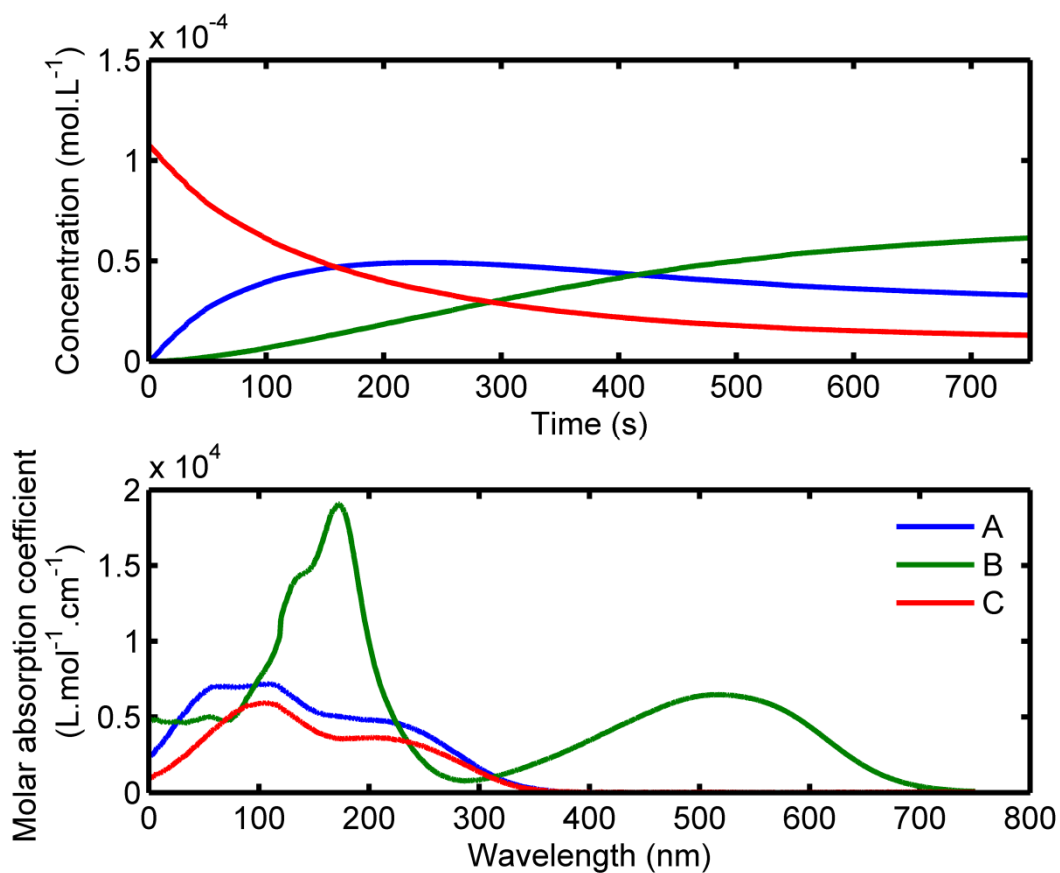


Fig. 3. Kinetic concentration profiles and absorption spectra for data corresponding to irradiation at 405 nm starting from C, obtained applying HS-MCR with the CMTE photochemical model, non-negativity on concentration and spectra and the closure constraints.

Figure 4

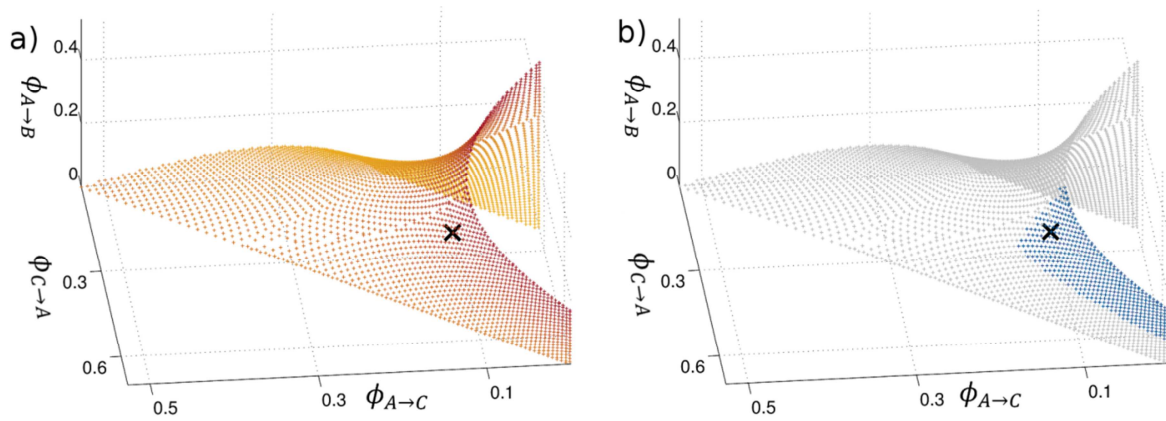


Fig. 4. Approximations of the sets K (a) and K^+ (b); the quantum yields ϕ_{opt} obtained by MCR are marked as black cross in the two plots. The shading of K is used for visualization purpose. The non-negativity constraint of the factor S was applied with a tolerance of 0.35% in order to reduce K to K^+ . The set K^+ is shown in blue color in the right plot. $\phi_{B \rightarrow A}$ is determined using the others quantum yields using the formula presented in the code in Appendix B (variable called v2).

Figure 5

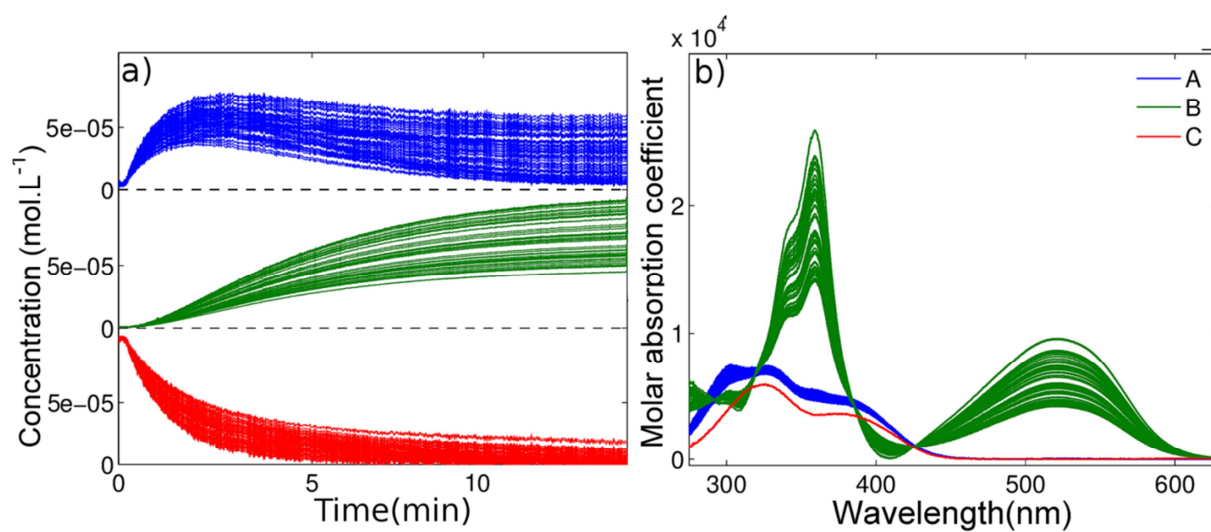


Fig. 5. Plots of the bands of a) concentration profiles and b) absorption spectra. The feasible factors C and S are evaluated for each representative of the set K^+ , which is shown in **Fig. 4**.

Figure 6

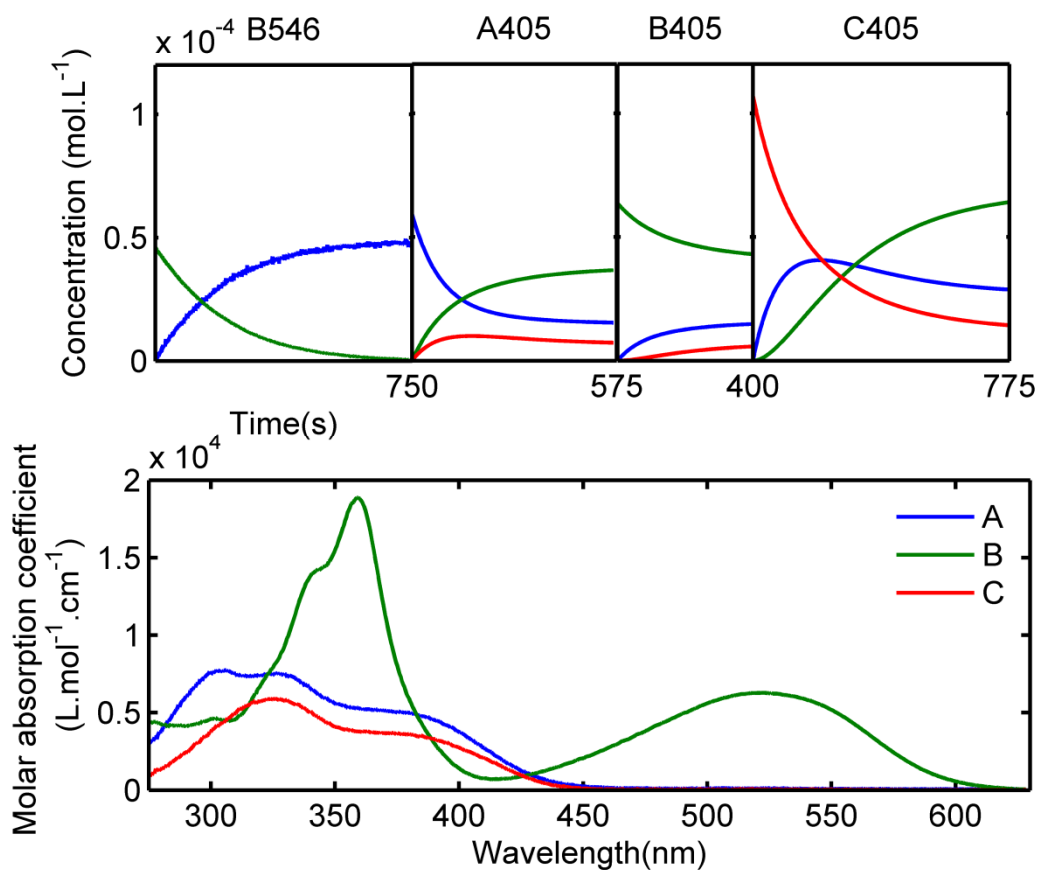


Fig. 6. HS-MCR results (top: concentration profiles, bottom: absorption spectra) for the multiset data [B546; A405; B405; C405]. The CMTE photochemical model was applied for the data at 405 nm. Only non-negativity of the concentrations and absorption spectra and closure constraints were applied for the data at 546 nm.

Figure 7

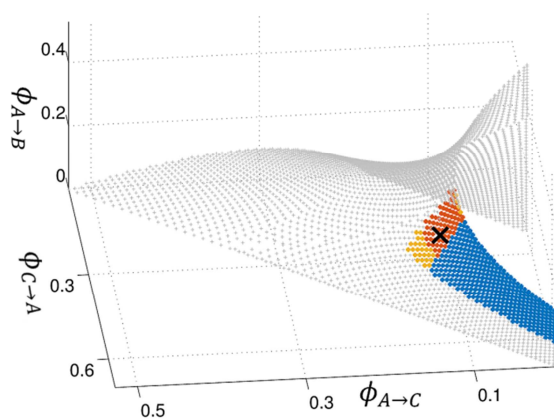


Fig. 7. Approximations of the set K^+ are shown for different multisets. First, the single data set C405 results in K^+ as shown in blue, yellow and red. The set K^+ for the multiset [A405; C405] is drawn in yellow and red. Finally, the largest multiset [A405; B405; C405] results in the smallest set K^+ (red). The quantum yield vector ϕ_{opt} obtained by HS-MCR is marked by a black cross.

Figure 8

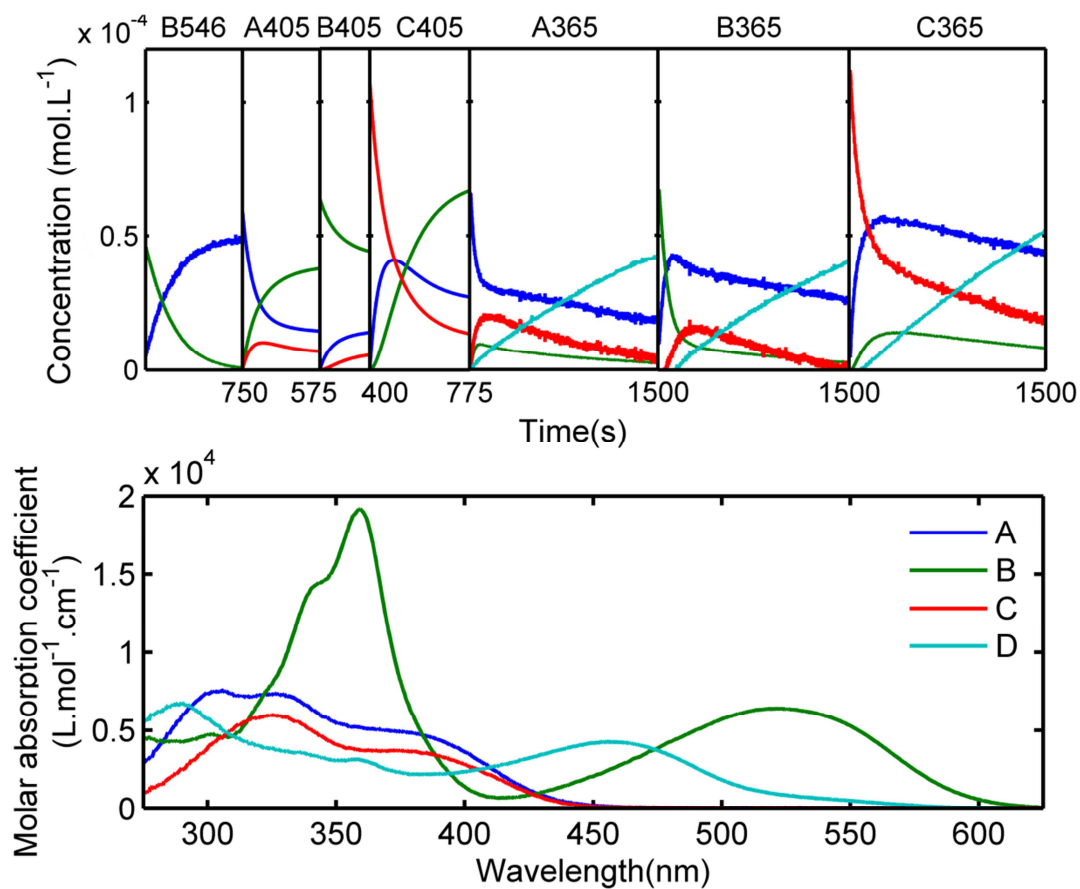


Fig. 8. HS-MCR results (top: concentration profiles, bottom: absorption spectra) for the multiset [B546; A405; B405; C405; A365; B365; C365]. The CMTE photochemical model was applied for the data at 405 nm. Only non-negativity of the concentrations and absorption spectra and closure constraints were applied for the data at 546 nm and 365 nm.

